applied sciences

MDPI

Article

A 2 μm Dual-Wavelength Laser at Cryogenic Temperature with Balanced Simultaneous Emission

Guangchao Ye, Wei Wang *, Haicheng Liu *, Wenqiang Xie, Shixing Xia, Qinggang Meng and Peng Lin

Heilongjiang Province Key Laboratory of Optoelectronics and Laser Technology, Heilongjiang Institute of Technology, Harbin 150050, China; yeguangchao@hljit.edu.cn (G.Y.)
* Correspondence: wangwei2@hljit.edu.cn (W.W.); liuhaicheng@hljit.edu.cn (H.L.)

Abstract: A Tm,Ho:YAP laser at cryogenic temperature is demonstrated for the first time with simultaneous emission at 2000 nm and 2119 nm. The feasibility of switching wavelength and achieving balanced output powers at two widely separated wavelengths has been confirmed by investigating the temperature dependence of the laser spectra. The optimal temperature for balanced output evidently diminishes as the pump power density increases, thereby manifesting a rate of change quantified at 1.19 K/W. At the optimal temperature of 43.1 K, the optical-to-optical conversion efficiency of the Tm,Ho:YAP simultaneous dual-wavelength laser (SDWL) with a pump power of 11.8 W is 12.7%, corresponding to a slope efficiency of 15.8%.

Keywords: dual-wavelength laser; Tm,Ho:YAP; cryogenic temperature; infrared lasers

1. Introduction

The simultaneous dual-wavelength laser (SDWL) [1] has been regarded for its applications in differential lidar [2–4], terahertz generation [5–7] and medical diagnosis [8–10]. The SDWL in a wavelength range around 2 μm holds great potential because of its human-eye safety and good transparency features [11–13].

Tm and Ho co-doped laser materials have been identified as prospective candidates for realizing a 2 μm SDWL because they possess many sharp fluorescent lines with the transitions of the splitting energy level in $^5I_7$ and $^5I_8$. Tm and Ho co-doped dual-wavelength fiber lasers operating at room temperature have been successfully demonstrated through the use of a cascaded fiber Bragg grating array [14] and a spatial filter [13]. In typical all-fiber dual-wavelength laser systems, the wavelength spacing is usually less than 10 nm.

Recently, a solid-state laser utilizing Tm,Ho:$GdYTaO_4$ crystal with a wavelength separation of 120 nm has been developed. Different lasing wavelengths and maximum output powers were realized by adjusting the concentration ratio of Tm and Ho ions [15]. Another work has demonstrated the feasibility and potential of using a Tm,Ho:YAG ceramic in diode-pumped dual-wavelength lasers, which can lead to high beam quality and high power density [16]. Moreover, recent research has reported a cryogenic SDWL operation of Tm:YLF using a modular setup around 2 μm. As the pump power increases, the output wavelength combination can transition from 1876 nm and 1901 nm to 1901 nm and 1912 nm [17].

However, there is a lack of sophisticated technological methodologies for the generation of 2 μm dual-wavelength solid-state lasers, which forces researchers to rely on specific laser crystals with particular doping concentrations or pumping powers to achieve simultaneous dual-wavelength output. Moreover, balancing the power ratio between the dual-wavelength components of the laser output remains a challenge for stable and consistent performance.

Currently, the growth techniques of Tm,Ho:YAP have become highly mature, and their structural anisotropy allows them to produce polarized emission spectra with multiple emission peaks, which provides strong support for the generation of multi-wavelength laser

Citation: Ye, G.; Wang, W.; Liu, H.; Xie, W.; Xia, S.; Meng, Q.; Lin, P. A 2 μm Dual-Wavelength Laser at Cryogenic Temperature with Balanced Simultaneous Emission. *Appl. Sci.* **2023**, *13*, 5750. https://doi.org/10.3390/app13095750

Academic Editor: Andrés Márquez

Received: 26 March 2023
Revised: 24 April 2023
Accepted: 4 May 2023
Published: 6 May 2023

oscillation. Li et al. founded that laser output with wavelengths of 2000 nm and 2119 nm can be achieved by Tm,Ho:YAP under CW and Q-switched modes, respectively [18]. However, achieving the simultaneous output of these two wavelengths has been a long-standing challenge.

For solid-state laser, the achievement of dual wavelength relies on controlling the gain and loss of different transition lines in the resonator to maintain a balance of net gain, thereby meeting the laser's threshold conditions. The threshold pump power is influenced by several factors, including the reflectivity of the output mirror, intracavity round-trip loss, the stimulated emission cross-section, and the overlap of pump and oscillating light. Thus, SDWL generation can be attained by regulating the aforementioned parameters.

Adjustment of the output mirror reflectivity can be achieved by applying a specific coating or utilizing an F-P filter as the output mirror, as demonstrated in previous studies [19,20]. For strongly gain-enhanced transition lines, the reflectivity of the output mirror at the two wavelengths needs to be determined based on the threshold conditions for dual-wavelength pumping, ensuring similar or equal threshold pump powers. For weakly gain-enhanced transition lines, it is essential to suppress the adjacent, strongly gain-enhanced transition lines. This ensures that the threshold pump power for the weakly gain-enhanced transition line is lower than that of the adjacent, strongly gain-enhanced transition line, ultimately facilitating dual-wavelength laser output. However, when the wavelengths of the dual-wavelength laser are close, controlling the threshold via coating becomes a major challenge.

For the design requirement of an SDWL with a small wavelength separation, the threshold pump power can be controlled by changing the intra-cavity losses of different wavelengths through the insertion of either an etalon or a birefringent filter within the resonant cavity [21,22]. Etalons are generally used for dual-wavelength lasers with frequency intervals smaller than 10 nm, while birefringent filters are more commonly used for dual-wavelength generation with frequency intervals of several tens of nanometers. However, since the method involves the insertion of elements to control losses, it may have some impact on the efficiency of the laser output.

Under fixed resonant cavity parameters, by altering the stimulated emission cross-sections, it is possible to control the threshold pump power at different wavelengths and thus achieve dual-wavelength laser emission. One approach to modifying the stimulated emission cross-sections is to change the angle between the laser propagation direction and the crystal axis, or to adjust the cooling temperature of the crystal [23–25]. The technique of achieving dual-wavelength lasers through cryogenic temperature tuning exploits the Stark splitting of the laser's upper and lower levels, which is induced by the unique lattice structure of the crystal. Further investigation of this technique shows potential for generating dual-wavelength lasers that are difficult to produce with conventional crystals, thus meeting the demands of various application scenarios.

In this work, we report for the first time a temperature-controlled cryogenic Tm,Ho:YAP laser with balanced output at 2000 nm and 2119 nm and conducted a detailed study of the dual-wavelength balancing process for the SDWL. This temperature-controlled gain balancing method for two resonant waves originating from transitions of different energy levels enables the use of a single, mature and reliable laser gain medium to achieve more universally applicable dual-wavelength laser outputs.

At an incident pump power of 11.8 W, a balanced output power of ∼1.51 W was generated, corresponding to an optical-to-optical conversion efficiency of 12.7% and a slope efficiency of 15.8%. Moreover, the beam-quality factors of the two wavelengths were $M^2_{2000} = 1.39$ and $M^2_{2119} = 1.30$, respectively. We experimentally obtained the optimal temperature for balancing the output powers of the two wavelengths. Considering the local heating effect from the pump absorption, the optimum temperature for the simultaneous dual-wavelength emission was experimentally found to vary with pump intensity.

2. Experimental Setup

The Tm,Ho:YAP laser crystals employed in this study were grown using the Czochralski technique at the Shanghai Institute of Optics and Fine Mechanics. The crystals were grown along the crystalline c-axis for $YAlO_3$, while the laser crystal sample containing 5 at.% thulium and 0.3 at.% holmium was cut along the α-axis. The crystal dimensions were measured to be 4 mm $\times$ 4 mm $\times$ 8 mm, with plane-parallel ends. Both end faces of the crystal were coated with a reflectivity of less than 0.5% at both 790–800 nm and 1.9–2.2 μm.

A schematic drawing of the laser setup used in these experiments is shown in Figure 1. A laser diode (nLight NL-PPS50-10030, Washington, DC, USA) with a maximum output power of 20 W and a central output wavelength of 794.1 nm was employed for pumping the Tm,Ho:YAP laser. The pump beam was coupled to a fiber with a core diameter of 100 μm and a numerical aperture of 0.22, and afterwards was re-focused on the crystal's center using collimation and focus lenses, both having focal lengths of 75 mm. A pump spot with a diameter of approximately 850 μm was placed on the center of the laser crystal with an overall coupling efficiency of approximately 80%. To ensure maximum laser output efficiency based on previous experimental results [18], we utilized a plane output coupler coated with partial reflectance (PR; R = 70%) for wavelengths ranging from 1.9 μm to 2.2 μm. Meanwhile, a plano-concave mirror with a 300 mm radius of curvature was used as the front mirror (M) with a high-transmittance coating (HT; T > 98.0%) at 790–798 nm as well as a high-reflective coating (HR; R > 99.5%) at 1.9–2.2 μm. The overall cavity length of the resonator was approximately 90 mm.

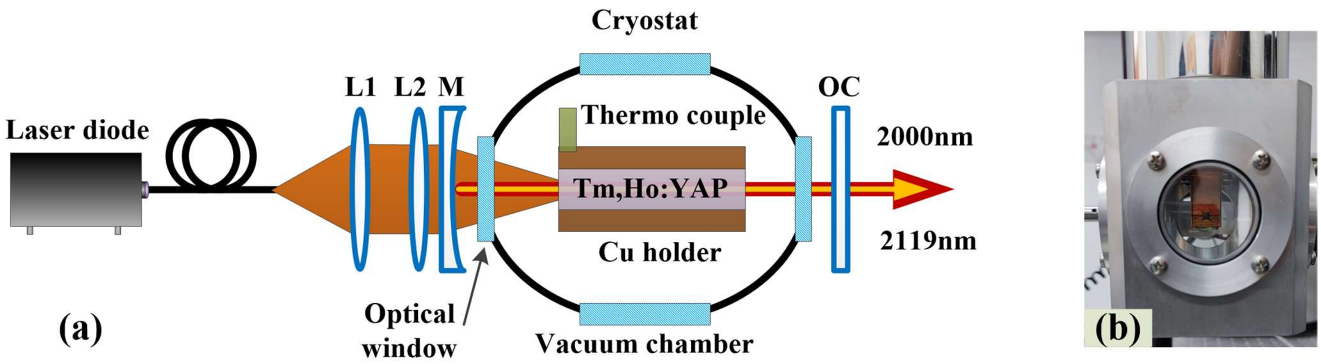

Figure 1. Experimental setup. (**a**) Schematic diagram of the Tm,Ho:YAP SDWL, with the temperature-controlled crystal mounted in an oxygen-free copper holder. (**b**) Photograph of the cryostat with a pair of plane-parallel optical windows.

The laser crystal was mounted in an oxygen-free copper holder with indium foil to improve the heat-spreading efficiency and was placed in a vacuum chamber. We attached the copper block to the cold finger of the temperature-controlled cryostat (Janis Research SHI-4-2, Woburn, MA, USA) with a temperature-control stability better than 0.05 K. A calibrated copper-constantan thermocouple was affixed directly to the crystal block to enable direct monitoring of temperature. Two plane-parallel optical windows coated with 99.5% transmittance at a wavelength of around 2 μm were placed in the vacuum chamber. The pressure gauge of the molecular pump indicated that the amount of vacuum was approximately 1.2×10^{-3} Pa, even though there was no accurate pressure sensor in the vacuum chamber.

3. Results

3.1. Laser Spectra

Initially, we investigated the temperature dependence of the laser spectra for the Tm,Ho:YAP crystal in order to gain a comprehensive understanding of the dual-wavelength output and the switching and balancing processes. The laser spectra were recorded using an optical spectrum analyzer (Horiba i550, Kyoto, Japan) with a 0.1 nm resolution.

As shown in Figure 2, when the pump power is maintained at approximately 5.0 W, precise temperature adjustment will alter the output wavelength of the laser. The laser wavelengths can switch between 2000 nm and 2119 nm, or simultaneously emit both wavelengths with varying intensity levels.

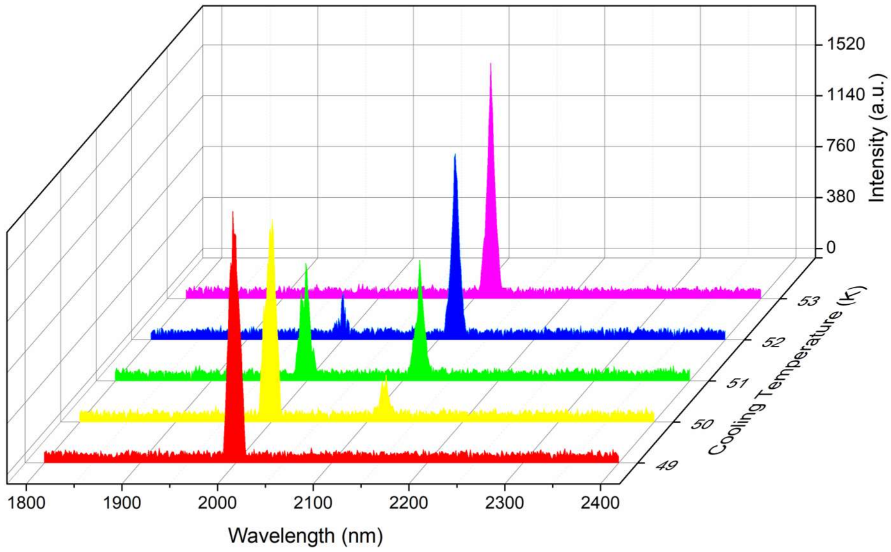

Figure 2. The switchable and intensity-controllable laser spectra.

At cryogenic temperatures, the Tm,Ho:YAP laser operates as a three-level system, where Tm^{3+} serves as a sensitizing ion. Tm^{3+} in $^3H_6$ (ground state) absorb pump light at 794.1 nm and transition to the excited-state $^3H_4$ level. Subsequently, they return to the $^3F_4$ level through a rapid cross-relaxation process. The energy of Tm^{3+} in $^3F_4$ level is similar in magnitude to that of Ho^{3+} in $^5I_7$. When the population of the $^3F_4$ level increases sharply, an energy-transfer process (ET: $Tm^{3+} + {}^3F_4 \leftrightarrow Ho^{3+} + {}^5I_7$) occurs between Tm^{3+} and Ho^{3+}, leading to a continuous increase in the population of Ho^{3+} at the $^5I_7$ level.

Once a population inversion is established between the excited state and the ground state of Ho^{3+}, a 2 μm laser can be achieved with $^5I_7$–$^5I_8$ transition. Finally, it should be noted that the generation of dual wavelengths is a result of the energy-level splitting that occurs in both $^5I_7$ and $^5I_8$, as indicated in Figure 3. Additionally, the population at the splitting energy level follows a Boltzmann distribution, with the Boltzmann occupancy factor changing with temperature. Therefore, the rate of spontaneous emission at 2119 nm increases with temperature, while the value at 2000 nm is reduced.

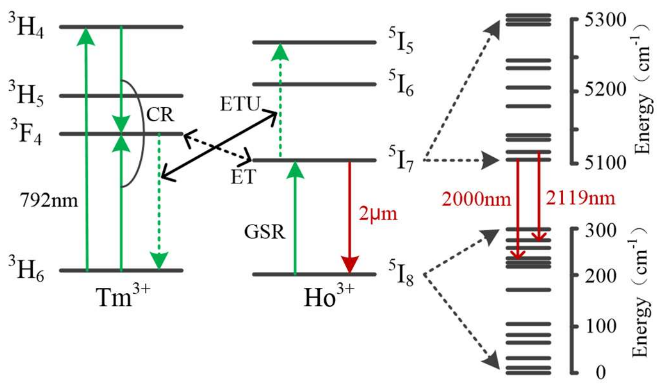

Figure 3. Schematic diagram of energy-level transitions and splitting in Tm,Ho:YAP crystals.

It is worth noting that although the laser crystal was cooled as a whole, the two laser wavelengths actually originated from different areas of the gain medium excited by the pump beam. As is well known, when longitudinal diode pumping is used, the temperature distribution inside the gain medium is typically non-uniform and Lorentzian-shaped. This suggests that the amount of fluorescence at the 2000 nm and 2119 nm wavelengths in Tm,Ho:YAP is not homogeneous, but rather depends on local temperature. Therefore, the rate of spontaneous emission at the 2119 nm wavelength is likely to be higher in the central part of the pump beam where the temperature is higher, whereas the rate of spontaneous emission at 2000 nm is superior in the surrounding area, where the temperature is lower.

According to the change process of the spectrum in Figure 2, prior to the temperature exceeding 49 K, there is only a single wavelength output of 2000 nm. However, as the temperature increases from 49 K to 53 K, the intensity of the 2000 nm wavelength component gradually diminishes, while the intensity of the 2119 nm wavelength component progressively augments. Once the temperature surpasses 53 K, only a single wavelength output of 2119 nm is present.

We believed that the optimal temperature for balanced output powers at two emission wavelengths was approximately 51 K, which was to be precisely determined in the following power measurement experiment. The spectral positions of these two components remained almost unchanged as the temperature increased, with the root-mean-square error of the peak position fluctuations for both wavelengths not exceeding 0.2 nm. This indicates that the wavelengths of the Tm,Ho:YAP SDWL under temperature control exhibit good stability, which would make them more suitable for use in gas-detection applications.

3.2. Output Power of the Tm,Ho:YAP SDWL

The spectral measurement results indicate that the power of each wavelength will change with temperature variation, and there should exist an optimal temperature point at which the output power of two wavelengths is equal. The signal transmission fiber and PbS detector of the spectrometer cannot guarantee a completely consistent intensity response for the two wavelengths. Consequently, the peak intensities of the laser spectrum cannot be used to accurately determine the power ratio of the dual wavelengths. Therefore, at this stage, a power meter was employed to conduct a detailed analysis of the balancing process for the SDWL.

The power meter used in the experiment was Coherent PM2, and, subsequently, the laser oscillation threshold with respect to incident pump power was found to be around 0.8 W. To explore the dynamics of the Tm,Ho:YAP SDWL, we utilized IR bandpass filters (T $\approx$ 0.04% at 2000 nm and T $\approx$ 61% at 2119 nm) to separate and record the output performance for each wavelength.

Figure 4 depicts the temperature dependence of the output powers at 2000 and 2119 nm for three different pump powers of 2.95 W, 4.98 W and 7.03 W. We determined optimal temperature values of approximately 52.7, 50.2 and 47.7 K, and obtained an SDWL with 0.03, 0.15 and 0.25 W output powers at both 2000 nm and 2119 nm.

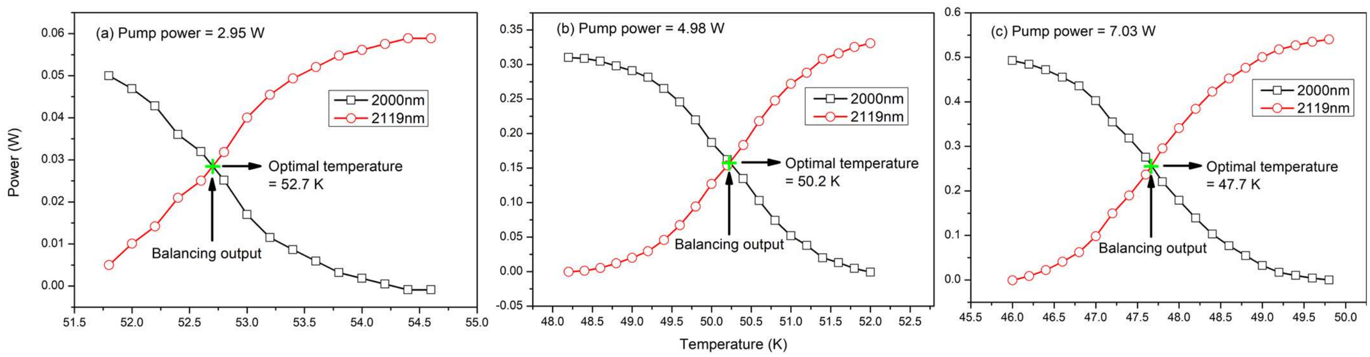

Figure 4. Output powers of the Tm,Ho:YAP SDWL at 2000 nm and 2119 nm with respect to the temperature at incident powers of (**a**) 2.95 W, (**b**) 4.98 W and (**c**) 7.03 W.

Furthermore, we also observed that the optimal temperature point is almost located at the central position of the dual-wavelength temperature-change process. Taking the dual-wavelength change process at a pump power of 4.98 W as an example, the critical temperature point for transitioning from a single 2000 nm wavelength output to a dual-wavelength output state is 48.2 K, and the critical temperature point for transitioning from a dual-wavelength output state to a single 2119 nm wavelength output is 52.1 K. The optimal temperature value required to achieve a balanced output is 50.2 K, which is approximately equal to the average of the two critical temperature values.

Based on the local heating generated by the pump absorption, it can be observed that the optimal temperature for achieving a balance in output powers at two distinct wavelengths depends on the pump power. Further investigations have reported optimal temperature values for various pump intensities, which provide confirmation of the influence of the local heating phenomenon, which is clearly demonstrated in Figure 5.

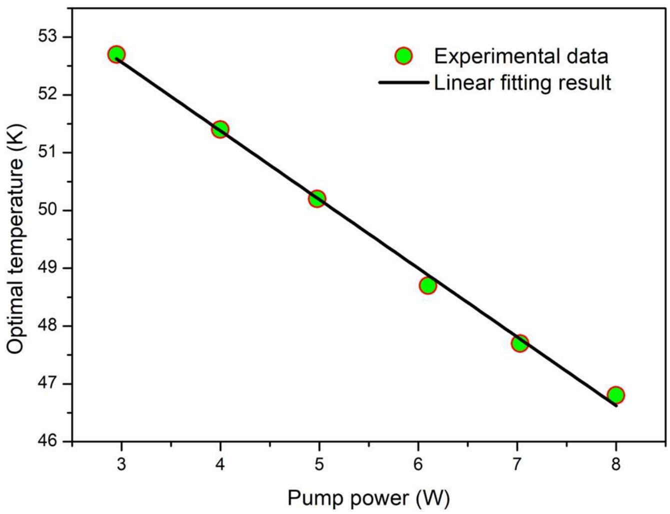

Figure 5. Experimental results of the optimal temperature for balanced output powers of two distinct wavelengths with respect to the pump power and the linear fitting curve of the experimental data.

It was observed that the optimal temperature for balancing the dual-wavelength output powers shifts toward lower values with increasing pump power due to the local heating. Empirical evidence suggests that the optimal temperature to achieve a balance in output powers at two distinct wavelengths exhibits an approximately linear relationship with the level of pump power. Furthermore, the rate of change of the optimal temperature with respect to the pump power can be estimated as 1.19 K/W.

Figure 6a shows the total SDWL output power in relation to temperature for different incident pump powers of 2.95, 4.98 and 7.03 W. It was observed that there was a slight improvement in overall performance as the temperature increased, and thus the overall output efficiency of the laser varies with temperature. Here, our primary focus is on the balanced output phenomenon at the optimal temperature; therefore, we calculated the output efficiency of the laser at the optimal temperature. According to Figure 6b, it can be calculated that at our maximal pump power of 11.8 W, the optical-to-optical conversion efficiency of the laser is 12.7%, and the slope efficiency was linearly fitted to be 15.8%.

3.3. Beam Quality and Power Stability

We conducted a further investigation of the beam quality of each wavelength of the Tm,Ho:YAP SDWL with balanced output at different pump powers (the optimal temperature values can be determined based on Figure 5). After performing a Gaussian transformation on the laser beam using a lens with a focal length of 100 mm, the two-dimensional laser profile of the beam waist was obtained by an infrared camera (Spiricon Pyrocam IIIHR, North Logan, UT, USA), and the beam quality of the SDWL was measured by a slit-scanning beam profiler (Thorlabs M2MS, Newto, NJ, USA).

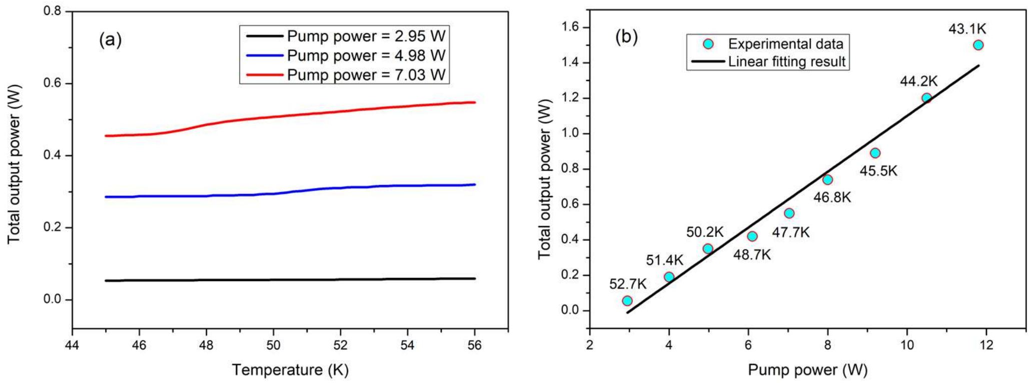

Figure 6. Total SDWL output power. (**a**) Temperature dependence of the output powers for different incident pump powers of 2.95, 4.98 and 7.03 W. (**b**) Output powers with respect to the pump powers at corresponding optimal temperatures (annotated alongside the data points in the graph).

Transverse distributions of the beam waist for the SDWL at 2000 nm and 2119 nm with pump powers of 2.95, 4.98, 6.10 and 7.03 W are illustrated in Figure 7a. The beam-profiling camera featured a 12.8 mm × 12.8 mm active area, and we specifically captured a central 1.5 mm × 1.5 mm region centered on the beam spot in the figure to offer a more detailed view of the beam's shape and distribution characteristics, showcasing subtle features and intensity variations. An integrated chopper was included in the camera setup to ensure the accuracy and reliability of the measurement for the 2 μm continuous-wave (CW) beams, effectively managing the beam's intensity and preventing potential sensor damage or saturation. The transverse beam cross-sections, which represent the spatial extent of the beam at specific wavelengths, were also measured. For wavelengths of 2000 nm and 2119 nm, we determined that the beam cross-sections were approximately 465 μm and 420 μm, respectively. As previously mentioned, the two wavelengths of laser actually originate from different areas of the gain medium excited by the pump beam. We found that the beam-waist radius of the 2000 nm wavelength component, which originates from the surrounding area of the gain medium, is overall slightly larger than that of the 2119 nm wavelength component, which comes from the central area of the gain medium. This results in the beam-quality M^2 factor of the 2119 nm wavelength component being slightly better than that of the 2000 nm wavelength component, as shown in Figure 7b. For any specific wavelength component, the beam-waist radius remains almost unchanged, while the beam-quality M^2 factor increases with the pump power. This indicates that the far-field divergence angle of the SDWL has expanded. With our maximal incident pump power of 11.8 W, the beam-quality factors of the two wavelengths were measured to be $M^2_{2000} = 1.39$ and $M^2_{2119} = 1.30$, respectively.

For a verification of the output stability, the dual-wavelength laser power was measured over 15 min, and the results are shown in Figure 8. The overall power level remained relatively stable, maintaining approximately 0.61 W. Although there was a slight drift in the output power of the two wavelength components, they consistently exhibited a complementary changing trend, such that when the power of one wavelength component increased, the power of the other wavelength component correspondingly decreased.

The root-mean-square-error (RMSE) power instabilities were slightly higher than those of the single-wavelength solid-state laser. The RMSEs of the total output power and the individual powers at 2000 nm and 2119 nm were 2.3%, 1.9% and 1.2%, respectively. These results indicate that the stability at 2000 nm is somewhat lower than that at 2119 nm, which is consistent with the relationship between beam quality and beam-waist radius. Compared with the previous results for a common dual-wavelength laser based on a single laser crystal [26,27], the power stabilities have been slightly improved.

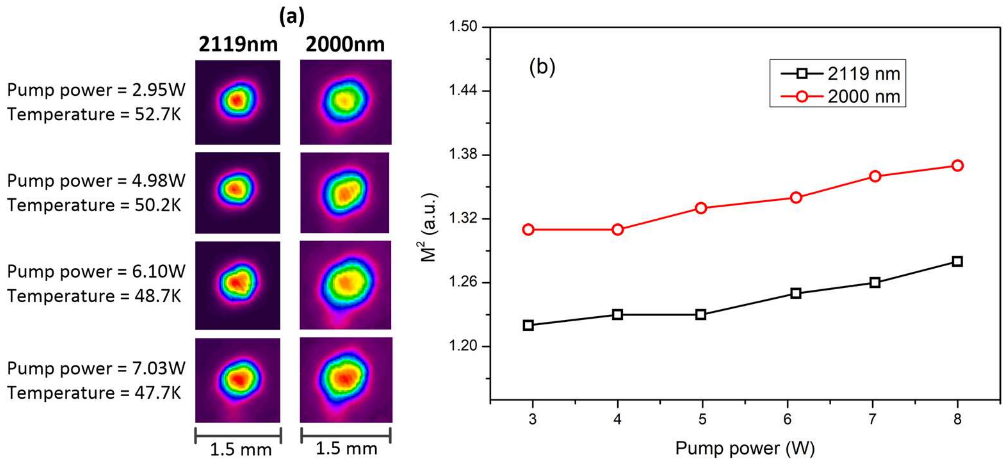

Figure 7. The beam quality of the Tm,Ho:YAP SDWL operated at optimal temperatures for balanced output. (**a**) Transverse distributions on beam waist and (**b**) M^2 factors for the SDWL at 2000 nm and 2119 nm with respect to the pump powers at corresponding optimal temperatures.

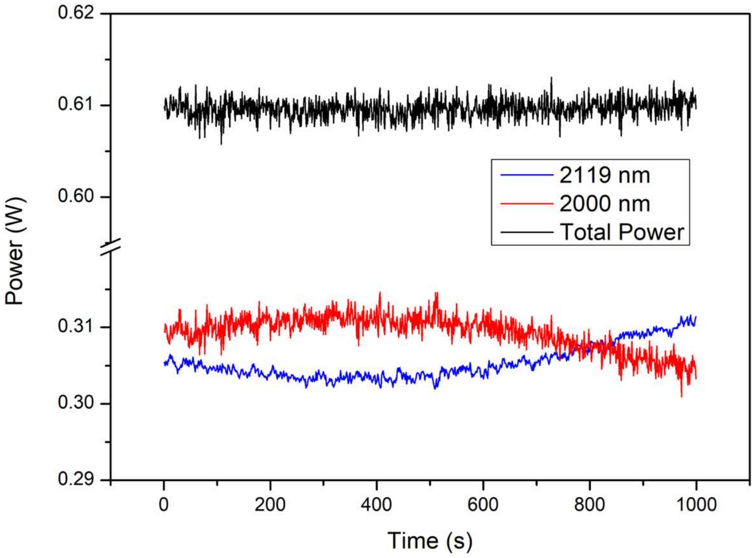

Figure 8. Dual-wavelength output power stability of the Tm,Ho:YAP SDWL.

4. Discussion

In light of the experimental results presented in this study, it is evident that the Tm,Ho:YAP SDWL demonstrates remarkable capabilities in terms of switchability and intensity-controllability. The switchability of the 2 μm laser is based on the influence of temperature on the stimulated emission cross-section, allowing the laser to work in stable dual-wavelength operation or switch between two wavelengths by adjusting the temperature controlled by the cryostat. The optimal temperature for balanced output will continuously decrease with increase in pump power, making temperature control at cryogenic temperatures crucial for achieving higher output power in the Tm,Ho:YAP SDWL. The method in this study may also potentially be applied to other SDWLs based on Tm and Ho ion doping.

Achieving balanced dual-wavelength laser output holds immense potential for advancement in multiple fields, including trace-gas detection, remote sensing and biomedical research. By enabling the simultaneous emission and precise control of two distinct wavelengths, these lasers offer new possibilities for innovation and technological development.

In future work, we will explore the implementation of Q-switching and mode-locking in the Tm,Ho:YAP SDWL. Moreover, based on fluorescence spectra from previous studies, the dual wavelength should exhibit π polarizations for 2000 nm and σ polarizations for 2119 nm. We plan to investigate the polarization characteristics of both wavelengths using suitable polarization beam splitters in subsequent studies. In this paper, the observed variations in total output power with temperature were likely related to the absorption spectra and absorption cross-sections of the laser crystal at different temperatures. We intend to conduct a detailed investigation of this aspect once an appropriate broadband light source becomes available. Based on the optimal temperature identified during the experiments, we will further investigate cost-effective, modular cooling solutions in order to develop a stable and user-friendly SDWL.

5. Conclusions

In conclusion, we have successfully demonstrated an efficient cryogenic Tm,Ho:YAP laser with simultaneous emission at two widely separated wavelengths. The feasibility of switching wavelength and achieving balanced output powers at 2000 nm and 2119 nm has been confirmed by investigating the temperature dependence of the laser spectra. Due to local heating arising from pump absorption, the optimal temperature for balanced output considerably decreases with increasing pump power density, with a rate of change of 1.19 K/W. At the optimal temperature of 43.1 K, the optical-to-optical conversion efficiency of the Tm,Ho:YAP SDWL with our maximal pump power of 11.8 W is 12.7%, corresponding to a slope efficiency of 15.8%. Moreover, the beam-quality factors of the two wavelengths are $M^2_{2000} = 1.39$ and $M^2_{2119} = 1.30$, respectively. To the best of our knowledge, this is the first time dual-wavelength balanced laser output has been achieved based on Tm,Ho:YAP crystals.

Author Contributions: Conceptualization and methodology, G.Y. and W.W.; validation, W.X.; investigation, S.X.; data curation, Q.M. and P.L.; writing, G.Y.; supervision, H.L.; project administration, W.W.; funding acquisition, G.Y. All authors have read and agreed to the published version of the manuscript.

Funding: This research was funded by the Natural Science Foundation of Heilongjiang Province, China, grant number LH2020F048.

Institutional Review Board Statement: Not applicable.

Informed Consent Statement: Not applicable.

Data Availability Statement: The data employed and/or studied in this research can be obtained from the corresponding author upon request.

Acknowledgments: This work was supported by the Xudong Li.

Conflicts of Interest: The authors declare no conflict of interest.

References

1. Zhu, H.Y.; Zhang, G.; Huang, C.H.; Wei, Y.; Huang, L.X.; Li, A.H.; Chen, Z.Q. 1318.8 nm/1338.2 nm simultaneous dual-wavelength Q-switched Nd:YAG laser. *Appl. Phys. B* **2008**, *90*, 451–454. [CrossRef]
2. Wang, C.-K.; Tseng, Y.-H.; Chu, H.-J. Airborne Dual-Wavelength LiDAR Data for Classifying Land Cover. *Remote Sens.* **2014**, *6*, 700–715. [CrossRef]
3. Cao, N.; Yang, S.; Cao, S.; Yang, S.; Shen, J. Accuracy calculation for lidar ratio and aerosol size distribution by dual-wavelength lidar. *Appl. Phys. A* **2019**, *125*, 590. [CrossRef]
4. Aoki, M.; Iwai, H. Dual-wavelength locking technique for coherent 2-m differential absorption lidar applications. *Appl. Opt.* **2021**, *60*, 4259–4265. [CrossRef]
5. Mei, J.; Zhong, K.; Wang, M.; Liu, P. High-Repetition-Rate Terahertz Generation in QPM GaAs With a Compact Efficient 2-μm KTP OPO. *IEEE Photonics Technol. Lett.* **2016**, *28*, 1501–1504. [CrossRef]
6. Pu, Z.; Ragam, S.; Ding, Y.J.; Zotova, I.B. Investigation of terahertz generation from passively Q-switched dual-frequency laser pulses. *Opt. Lett.* **2011**, *36*, 4818–4820. [CrossRef]
7. Zhong, K.; Shi, W.; Degang, X.U.; Liu, P.X.; Wang, Y.Y.; Mei, J.L.; Yan, C.; Shijie, F.U.; Yao, J.Q.; University, T. Optically pumped terahertz sources. *Sci. China* **2017**, *60*, 1801–1818. [CrossRef]
8. Nguyen, H.; Steenbergen, W. Feasibility of identifying reflection artifacts in photoacoustic imaging using two-wavelength excitation. *Biomed. Opt. Express* **2020**, *11*, 5745–5759. [CrossRef]

9. Negishi, K.; Akita, H.; Matsunaga, Y. Prospective study of removing solar lentigines in Asians using a novel dual-wavelength and dual-pulse width picosecond laser. *Lasers. Surg. Med.* **2018**, *50*, 851–858. [CrossRef]
10. Wang, T.; Da, C.; Yang, J.; Gang, M.; Lin, X. Safety and Efficacy of Dual Wavelength Laser (1064 nm + 595 nm) for Treatment of non-treated port-wine stains. *J. Eur. Acad. Dermatol. Venereol.* **2017**, *32*, 260–264. [CrossRef]
11. Queißer, M.; Burton, M.; Fiorani, L. Differential absorption lidar for volcanic CO_2 sensing tested in an unstable atmosphere. *Opt. Express* **2015**, *23*, 6634–6644. [CrossRef] [PubMed]
12. Yao, B.Q.; Shen, Y.J.; Duan, X.M.; Dai, T.Y.; Ju, Y.L.; Wang, Y.Z. A 41-W ZnGeP2 optical parametric oscillator pumped by a Q-switched Ho:YAG laser. *Opt. Lett.* **2014**, *39*, 6589–6592. [CrossRef] [PubMed]
13. Geng, J.; Jiang, S. Fiber Lasers: The 2 µm Market Heats Up. *Opt. Photonics News* **2014**, *25*, 34–41. [CrossRef]
14. Zhou, P.; Wang, X.L.; Ma, Y.X.; Han, K.; Liu, Z.J. Stable all-fiber dual-wavelength thulium-doped fiber laser and its coherent beam combination. *Laser Phys.* **2011**, *21*, 184–187. [CrossRef]
15. Wang, B.; Gao, C.; Dou, R.; Nie, H.; Sun, G.; Liu, W.; Yu, H.; Wang, G.; Zhang, Q.; Lin, X.; et al. Dual-wavelength mid-infrared CW and Q-switched laser in diode end-pumped Tm,Ho:$GdYTaO_4$ crystal. *Laser Phys. Lett.* **2018**, *15*, 025801. [CrossRef]
16. Liu, P.; Jin, L.; Liu, X.; Huang, H.; Zhang, J.; Tang, D.; Shen, D. A Diode-Pumped Dual-Wavelength Tm, Ho: YAG Ceramic Laser. *IEEE Photonics J.* **2016**, *8*, 1–7. [CrossRef]
17. Alles, A.; Jambunathan, V.; Slimi, S.; Serres, J.M.; Aguiló, M.; Díaz, F.; Mateos, X.; Smrz, M.; Mocek, T. Cryogenic Tm:$LiYF_4$ laser around 2 µm. *Appl. Phys. B* **2023**, *129*, 41. [CrossRef]
18. Li, L.; Yang, X.; Zhou, L.; Xie, W.; Wang, Y.; Shen, Y.; Yang, Y.; Yang, W.; Wang, W.; Lv, Z.; et al. Active/passive Q-switching operation of 2 µm Tm,Ho:YAP laser with an acousto-optical Q-switch/MoS2 saturable absorber mirror. *Photonics Res.* **2018**, *6*, 614–619. [CrossRef]
19. Shang, L.H.; Wen, Y.; Li, T.Y.; Guo, Y.Y.; Wang, Y.H.; Wu, C.T.; Wang, C.; Jin, G.Y. Pulse peaks synchronize dual-wavelength laser based on Q-switch delay trigger. *Infrared Phys. Technol.* **2021**, *116*, 103751. [CrossRef]
20. Han, S.; Zhou, S.; Liu, X.; Yan, Q.; Zhang, S. Rhenium disulfide-based passively Q-switched dual-wavelength laser at 0.95 mu m and 1.06 mu m in Nd:YAG. *Laser Phys. Lett.* **2018**, *15*, 085804. [CrossRef]
21. He, J.; Wei, F.; Liu, H.; Xia, J.; Yang, R.; Lu, Y. Tunable continuous-wave dual-wavelength laser operation of Pr3+:LiYF4 around 900 nm. *Laser Phys. Lett.* **2021**, *18*, 085003. [CrossRef]
22. Gao, C.; Lv, S.; Zhu, G.; Wang, G.; Su, X.; Wang, B.; Kumar, S.; Dou, R.; Peng, F.; Zhang, Q.; et al. Self-Q-switching and passively Q-switched mode-locking of dual-wavelength Nd:YSAG laser. *Opt. Laser Technol.* **2020**, *122*, 105860. [CrossRef]
23. Smirnov, I.V.; Zverev, P.G.; Sirotkin, A.A. Efficient multiwavelength operation of a diode-pumped Nd:$YAlO_3$ laser at 1064, 1072 and 1079 nm. *Laser Phys. Lett.* **2020**, *17*, 095001. [CrossRef]
24. Cho, C.Y.; Tuan, P.H.; Yu, Y.T.; Huang, K.F.; Chen, Y.F. A cryogenically cooled Nd:YAG monolithic laser for efficient dual-wavelength operation at 1061 and 1064 nm. *Laser Phys. Lett.* **2013**, *10*, 045806. [CrossRef]
25. Cho, C.Y.; Huang, T.L.; Wen, S.M.; Huang, Y.J.; Huang, K.F.; Chen, Y.F. Nd:YLF laser at cryogenic temperature with orthogonally polarized simultaneous emission at 1047 nm and 1053 nm. *Opt Express* **2014**, *22*, 25318–25323. [CrossRef]
26. Zuo, Z.Y.; Dai, S.B.; Zhu, S.Q.; Yin, H.; Chen, Z.Q. Power scaling of an actively Q-switched orthogonally polarized dual-wavelength Nd:YLF laser at 1047 and 1053 nm. *Opt. Lett.* **2018**, *43*, 4578–4581. [CrossRef]
27. Zhong, K.; Mei, J.; Wang, M. Compact High-Repetition-Rate Monochromatic Terahertz Source Based on Difference Frequency Generation from a Dual-Wavelength Nd:YAG Laser and DAST Crystal. *J. Infrared Millim. Terahertz Waves* **2017**, *38*, 87–95. [CrossRef]